

# Towards a reliable, automated method of individual alpha frequency (IAF) quantification

Andrew W. Corcoran<sup>a,b</sup>, Phillip M. Alday<sup>b,c</sup>,

Matthias Schlesewsky<sup>b</sup>, Ina Bornkessel-Schlesewsky<sup>b</sup>

<sup>a</sup>Cognition and Philosophy Laboratory, Monash University, Melbourne, Australia.

<sup>b</sup>Centre for Cognitive and Systems Neuroscience, University of South Australia, Adelaide, Australia.

<sup>c</sup>Max Planck Institute for Psycholinguistics, Nijmegen, 6500 AH, The Netherlands.

**Correspondence** A.W. Corcoran, Cognition and Philosophy Laboratory, Room E672, Menzies Building, 20 Chancellors Walk, Monash University, Clayton, VIC 3800, Australia.

Email: [andrew.corcoran1@monash.edu](mailto:andrew.corcoran1@monash.edu)

Telephone: +61 (3) 9905 9166

**Funding** This work was partially supported by funding from the University of South Australia Ehrenberg-Bass Institute for Marketing Science. This funding supported AWC while he collected and analysed the empirical EEG dataset reported in this manuscript. The Institute had no influence on the design, analysis, or interpretation of the reported study. AWC is supported by an Australian Government Research Training Program Scholarship. IBS is supported by an Australian Research Council Future Fellowship (FT160100437).

## Abstract

20  
21 Individual alpha frequency (IAF) is a promising electrophysiological marker of interindividual differences  
22 in cognitive function. IAF has been linked with trait-like differences in information processing and general  
23 intelligence, and provides an empirical basis for the definition of individualised frequency bands. Despite its  
24 widespread application, however, there is little consensus on the optimal method for estimating IAF, and  
25 many common approaches are prone to bias and inconsistency. Here, we describe an automated strategy for  
26 deriving two of the most prevalent IAF estimators in the literature: peak alpha frequency (PAF) and centre of  
27 gravity (CoG). These indices are calculated from resting-state power spectra that have been smoothed using a  
28 Savitzky-Golay filter (SGF). We evaluate the performance characteristics of this analysis procedure in both  
29 empirical and simulated EEG datasets. Applying the SGF technique to resting-state data from  $n = 63$  healthy  
30 adults furnished 61 PAF, and 62 CoG estimates. The statistical properties of these estimates were consistent  
31 with previous reports. Simulation analyses revealed that the SGF routine was able to reliably extract target  
32 alpha components, even under relatively noisy spectral conditions. The routine consistently outperformed a  
33 simpler method of automated peak detection that did not involve spectral smoothing. The SGF technique is  
34 fast, open-source, and available in two popular programming languages (MATLAB and Python), and thus can  
35 easily be integrated within the most popular M/EEG toolsets (EEGLAB, FieldTrip and MNE-Python). As  
36 such, it affords a convenient tool for improving the reliability and replicability of future IAF-related research.

37

38 **Keywords:** Alpha Rhythm, EEG, Oscillation/Time Frequency Analyses, Savitzky-Golay Filter, Individual  
39 Alpha Frequency

## 40 1 Introduction

41 Alpha is the dominant rhythm in the human EEG, and its importance for cognitive processing has been  
42 recognised since Hans Berger’s seminal work in the early 20th century (cf. Adrian & Matthews, 1934; Berger,  
43 1929). Interindividual differences in the predominant frequency of alpha-band oscillations (i.e. individual alpha  
44 frequency; IAF) have been linked with variability in cognitive performance since the 1930s (for a more recent  
45 review, see Klimesch, 1999; see Vogel & Broverman, 1964). More recent research has revealed that IAF predicts  
46 performance on a variety of perceptual (e.g., Cecere, Rees, & Romei, 2015; Samaha & Postle, 2015) and  
47 cognitive (e.g., Bornkessel, Fiebach, Friederici, & Schlesewsky, 2004; Klimesch, Doppelmayr, & Hanslmayr,  
48 2006) tasks. Individuals with a low IAF process information more slowly (Klimesch, Doppelmayr, Schimke,  
49 & Pachinger, 1996; Surwillo, 1961, 1963), and show reduced performance on memory tasks (Klimesch, 1999)  
50 and general intelligence measures ( $g$ ; Grandy et al., 2013a), in comparison to their high-IAF counterparts.  
51 IAF is a trait-like characteristic of the human EEG (Grandy et al., 2013b), which shows high heritability  
52 (Lykken, Tellegen, & Thorkelson, 1974; Malone et al., 2014; Smit, Wright, Hansell, Geffen, & Martin, 2006) and  
53 test-retest reliability (Gasser, Bächer, & Steinberg, 1985; Kondacs & Szabo, 1999; Näpflin, Wildi, & Sarnthein,  
54 2007). However, IAF tends to decrease with age from young adulthood onwards (Chiang, Rennie, Robinson,  
55 Albada, & Kerr, 2011; Köpruner, Pfurtscheller, & Auer, 1984), hence lifelong changes in IAF accompany  
56 the decline of many cognitive abilities in older adulthood (e.g. Hedden & Gabrieli, 2004; Salthouse, 2011).  
57 Taken together, this evidence highlights the utility of the IAF as a neurophysiological marker of general brain  
58 functioning (Grandy et al., 2013a, 2013b).

59 In addition to quantifying individual differences in the properties of the dominant alpha rhythm, IAF can also  
60 be used to derive individualised estimates of the canonical frequency bands beyond alpha (Klimesch, 2012).  
61 Such empirically-driven approaches to frequency band definition have been proposed to sharpen the precision  
62 of frequency-domain analyses more generally (Klimesch, 2012). Indeed, using the IAF to distinguish subregions  
63 of the alpha band has revealed functional dissociations between lower- and higher-frequency alpha-rhythms  
64 (e.g., Klimesch, 1997). However, despite the potential advantages of deploying the IAF as a reference point for  
65 various kinds of individualised spectral analysis, no clear consensus on the optimal method for quantifying IAF  
66 currently exists. This paper thus sets out to develop a rigorous, automated strategy for estimating two of the  
67 most widely reported indices of IAF: peak alpha frequency (PAF) and alpha frequency centre of gravity (CoG).  
68 We begin by briefly describing some of the most common strategies for extracting these estimators, and their  
69 attendant problems.

## 70 **1.1 Peak alpha frequency**

71 IAF estimation typically depends on the delineation of a singular, prominent spectral peak within the alpha  
72 bandwidth (standardly defined as 8-13 Hz; Noachtar et al., 2004). In many cases, the PAF can be easily  
73 discerned upon visual inspection of the power spectral density (PSD) from eyes-closed resting-state EEG  
74 recorded over parieto-occipital sites. However, this strategy is complicated by the presence of two (or more)  
75 alpha-band peaks (so-called “split-peaks”; Chiang et al., 2011), or the lack of any obvious deviation from the  
76 characteristic  $1/f$ -like scaling of background M/EEG spectral activity (the “inverse power-law”; Pritchard,  
77 1992). Under such circumstances, subjective PAF estimation may be prone to bias and inconsistency (Chiang  
78 et al., 2008), thus posing a significant challenge to replicability. While conservative approaches to PAF  
79 identification in the context of ambiguous spectral conditions may help reduce bias, this may result in high  
80 rates of attrition (see for e.g., Bornkessel-Schlesewsky et al., 2015).

81 One approach for improving the objectivity, replicability, and (for larger datasets) practicality of PAF estimation  
82 is to implement an automated peak-detection algorithm. While this strategy does not solve the basic problem  
83 of deciding the criteria by which valid PAF estimates are discriminated from split-peaks or spurious background  
84 fluctuations, it at least applies such criteria consistently across all subjects. Simple algorithms may however  
85 introduce new sources of bias. For instance, a basic routine that searches for local maxima within the alpha  
86 band may arbitrarily assign the PAF to the lower bound of the search window in the absence of any notable  
87 deviation from the inverse-power law (since the highest power estimate will be the supremum found at the  
88 lowest frequency bin spanned by the window). A more sophisticated approach such as the first-derivative test  
89 (in which the first derivative of the PSD is searched for downward going zero crossings; cf. Grandy et al., 2013b)  
90 avoids this problem, but is still incapable of distinguishing substantive peaks from split-peaks or arbitrarily  
91 small deviations from background spectral activity. Such routines may therefore be too liberal with regard to  
92 the spectral features they classify as alpha peaks.

## 93 **1.2 Alpha-band centre of gravity and reactivity**

94 The alpha mean or CoG frequency (Klimesch, Schimke, Ladurner, & Pfurtscheller, 1990) has been proposed as  
95 an alternative method of IAF estimation that circumvents some of the difficulties posed by the absence of a  
96 dominant alpha peak (Klimesch, 1997; Klimesch, Schimke, & Pfurtscheller, 1993). This estimator computes a  
97 weighted average of the power contained within the alpha-band, thus rendering a summary measure that is  
98 sensitive to the spectral distribution of alpha components. Given that the span and location of alpha-rhythm  
99 activity vary across individuals (Bazanov & Vernon, 2014), Klimesch and colleagues (1990) recommended

100 computing the CoG using bespoke frequency windows designed to capture such variation. However, the  
101 definition of such individualised alpha-band windows (IAWs) poses a nontrivial challenge, and may rely on  
102 subjective assessments or arbitrary criteria (Bazanov & Vernon, 2014). One principled solution to this problem  
103 is to derive the IAW from reactivity-based contrasts between two conditions (pre- vs. peri-stimulus presentation,  
104 Goljahani et al., 2012; e.g., eyes-closed vs. eyes-open resting-states, Klimesch, 1999). This approach is not  
105 immune to bias, however, since alpha rhythms are not always substantially attenuated by opening the eyes  
106 (Gaál, Boha, Stam, & Molnár, 2010; Kreitman & Shaw, 1965), and may only be partially attenuated (e.g.,  
107 Klimesch et al., 2006) – or even *enhanced* (e.g., Rihs, Michel, & Thut, 2007) – during experimental tasks.

### 108 **1.3 Curve-fitting approaches to alpha-rhythm quantification**

109 One promising approach to spectral peak quantification that avoids many of the issues highlighted above applies  
110 iterative curve-fitting techniques to parameterise the statistical properties of the PSD (e.g., Chiang et al., 2008;  
111 Lodder & Putten, 2011). The practical utility of such methods is clearly apparent from their application to  
112 large  $n$  datasets (Albada & Robinson, 2013; e.g., Chiang et al., 2011), while comparison of Lodder and van  
113 Putten’s (2011) algorithm with human scorers revealed a high degree of estimator agreement. It is puzzling  
114 then why such methods have not been taken up more broadly within the IAF literature (cf. Haegens, Cousijn,  
115 Wallis, Harrison, & Nobre, 2014, for a notable exception). One possibility is that investigators are generally  
116 unaware of these approaches, given that they have mostly been applied in the context of spectral modeling  
117 rather than IAF research (nor Bazanova and Vernon, 2014, mention the existence of such methods in their  
118 reviews of IAF estimation techniques; indeed, neither Goljahani et al., 2012). Alternatively, investigators may  
119 be put off by the perceived burden involved in accessing these programmes (which we have not been able to  
120 locate publically) and integrating them within existing analysis pipelines (which may not be compatible with  
121 such algorithms). We suggest then that one of the critical steps towards achieving a more widespread adoption  
122 of automated IAF estimators is to make these tools openly available in formats that can be easily assimilated  
123 within popular methods of M/EEG analysis.

### 124 **1.4 Aims of the present study**

125 In sum, common methodological approaches to IAF estimation are either (1) time-consuming and vulnerable to  
126 inconsistencies arising from subjective evaluation, or (2) at risk of producing spurious or biased estimates under  
127 certain plausible spectral conditions. More recent innovations that address these problems via the application  
128 of sophisticated curve-fitting algorithms have so far found limited uptake within the broader IAF literature,

129 perhaps on account of practical barriers pertaining to software access and implementation. Consequently,  
130 we sought to develop an automated method of alpha-band quantification that provides fast, reliable, and  
131 easily replicated estimates of the resting-state IAF in two major programming languages: MATLAB® (The  
132 MathWorks, Inc., Natick, MA, USA) and Python™. This goal is consistent with recent proposals to make the  
133 analysis of electrophysiological data as open, transparent, and amenable to replication as possible (Cohen,  
134 2017).

## 135 **2 Method**

136 Our approach aims to emulate Klimesch and colleagues' (1990) original attempt to characterise individual  
137 profiles of resting-state alpha-band activity by means of a relatively simple, non-parametric curve-fitting  
138 technique; the Savitzky-Golay filter (SGF). The basic strategy runs as follows: First, we extract PSD estimates  
139 from preprocessed, fast Fourier-transformed EEG signals. Second, we apply the SGF to smooth the PSD  
140 function and estimate its first- and second-order derivatives. Third, these derivatives are analysed for evidence  
141 of a distinct spectral peak within the alpha band region. Finally, the first derivative of the PSD is reanalysed  
142 to locate the bounds of the IAW, from which the CoG is estimated. Our main focus here will be to assess the  
143 efficacy of this approach in the context of both empirical and simulated data. For a more rigorous account of  
144 the calculations implemented in the algorithm, see Appendix.

### 145 **2.1 Savitzky-Golay smoothing and differentiation**

146 The SGF is a least-squares polynomial curve-fitting procedure specifically designed to aid the detection of  
147 spectral peaks amidst noisy conditions (Savitzky & Golay, 1964). The major advantage of the SGF in this  
148 regard is its ability to smooth peaks while preserving their height, width, position, and CoG (Schafer, 2011;  
149 see Ziegler, 1981). Consequently, we propose using the SGF in order to attenuate random fluctuations in the  
150 PSD (and thus improve signal-to-noise ratio; SNR) without substantially distorting the spectral parameters  
151 of interest in IAF analysis. Eliminating such fluctuations should reduce the number of spurious local optima  
152 in the derivatives of the PSD, thus improving the overall accuracy and reliability of the first-derivative test.  
153 Conveniently, SGFs constitute optimal (or near optimal) differentiators (Luo, Ying, He, & Bai, 2005), and  
154 hence can be deployed to estimate both the smoothed PSD and its derivatives simultaneously.

## 155 2.2 Implementation

156 All functions developed in order to conduct the analyses reported here are open-source and available (along  
157 with sample datasets and simulation materials) from <https://github.com/corcorana/restingIAF>. The following  
158 report focuses on the MATLAB implementation of the algorithm, which is dependent on the Signal Processing  
159 Toolbox™ and EEGLAB (Delorme & Makeig, 2004). The pipeline (Figure 1) relies on MATLAB’s `pwelch`  
160 implementation of Welch’s modified periodogram method (Welch, 1967) to derive PSD estimates. This requires  
161 the selection of a sliding window function of  $x$  length, which determines the frequency resolution of the analysis.  
162 (Note, alternative methods of PSD estimation could be coupled with the SGF routine, but are not explored  
163 here.) The following parameters must also be specified in order to execute the algorithm (examples of what we  
164 consider to be reasonable values are outlined in Section 2.3.4):

- 165 •  $F_w$ , SGF frame width (longer = more smoothing; Bromba & Ziegler, 1981);
- 166 •  $k$ , SGF polynomial degree (higher = less smoothing/peak height loss; Press, Teukolsky, Vetterling, &  
167 Flannery, 1992);
- 168 •  $W_\alpha$ , the domain of the PSD searched for evidence of peak activity;
- 169 •  $minP$ , the minimum power value that a local maximum must exceed to qualify as a peak candidate  
170 (defined as 1 s.d. above the power estimate predicted by a regression model of the log-transformed PSD);
- 171 •  $pDiff$ , the minimum proportion of peak height by which the highest peak candidate within  $W_\alpha$  must  
172 exceed any competitors to be assigned as the PAF;
- 173 •  $cMin$ , the minimum number of channel estimates necessary for computing cross-channel averages.

174 Since channel spectra may be differentially contaminated by signal noise, our algorithm evaluates the relative  
175 ‘quality’ of channel-wise PAF estimates prior to cross-channel averaging. To this end, we extend the logic  
176 of the first-derivative test to extract second derivative estimates of the inflection points bounding the PAF.  
177 These points are used to define the area under the peak (normalised power units), which is then divided by the  
178 frequency span of this area. The resulting quantity ( $Q$  value) thus affords an indication of the relative quality of  
179 the resolved peak in terms of how well its distributional characteristics conform to the ideal of a highly powered,  
180 less variable (i.e. narrower) peak (as opposed to broader and/or shallower counterparts). Within-subject channel  
181 estimates are scaled in proportion to the peak with the highest  $Q$  value, and the (weighted) cross-channel  
182 average computed (hence, channels with the strongest evidence of PAF detection contribute more information  
183 to the mean estimate of the PAF). We consider this strategy (which only influences results when channel  
184 estimates fail to converge) an acceptable trade-off between loss of information (incurred by higher rates of  
185 channel exclusion) vs. loss of precision (incurred by treating all estimates as equally indicative of the estimand).

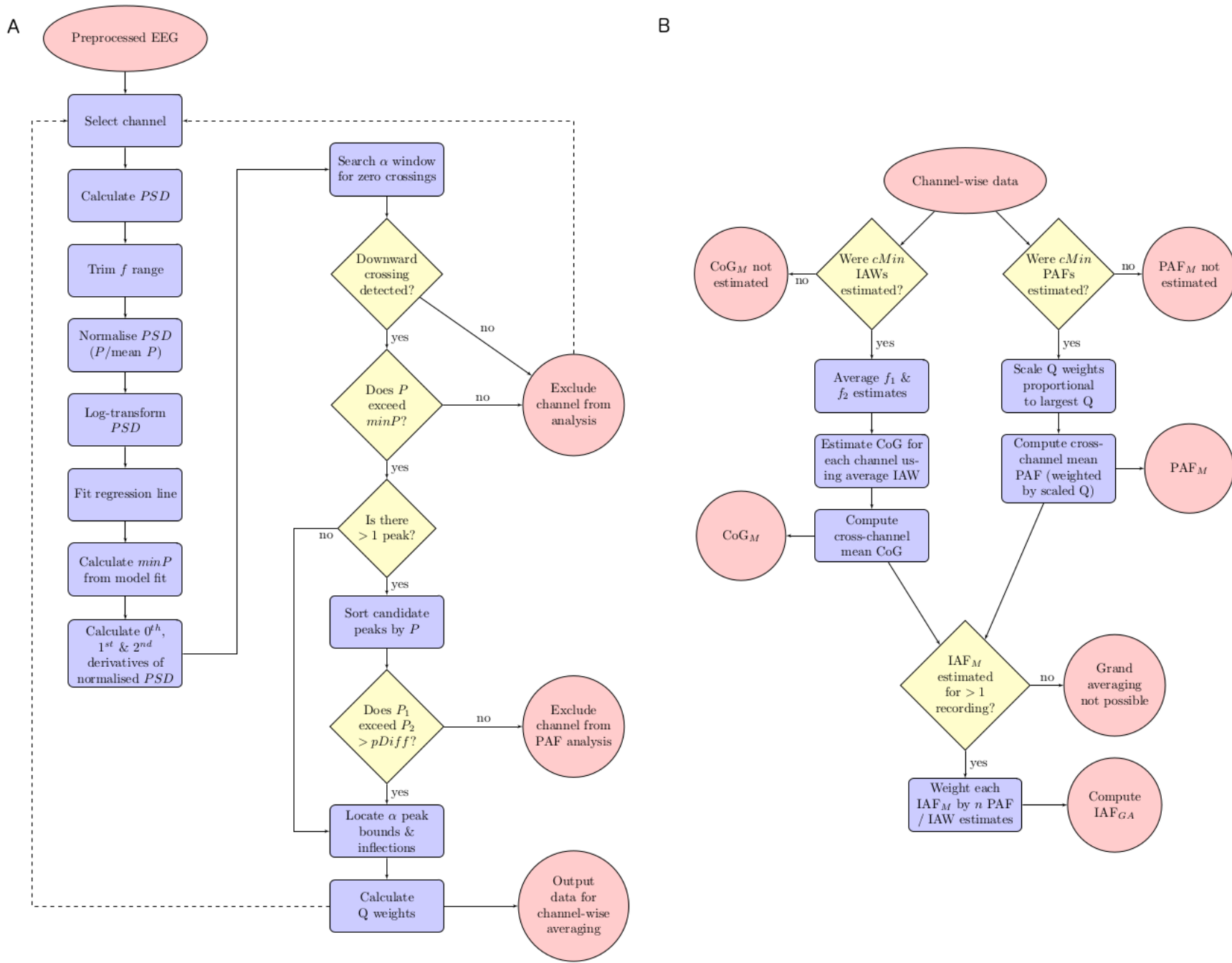


Figure 1: Flow diagrams summarising key steps of the analysis pipeline. (A) depicts processing of channel data, (B) depicts cross-channel averaging, assuming a sufficient number of estimates. See main text/Appendix for details. *PSD*: power spectral density; *f range*: frequency bins included in analysis; *P*: power estimate; *minP*: minimum power necessary to qualify as a candidate peak; *pDiff*: minimum power difference necessary to qualify as a PAF estimate; *Q weights*: quantification of relative peak quality (scaled *Q* value); *cMin*: minimum number of channel estimates required for cross-channel averaging; *IAW*: individualised alpha-band window;  $f_1$  and  $f_2$ : lower and upper bounds of IAW;  $PAF_M$ : mean PAF estimate;  $CoG_M$ : mean CoG estimate;  $IAF_M$ :  $PAF_M$  or  $CoG_M$ ;  $IAF_{GA}$ : grand average PAF/CoG estimate.

## 186 **2.3 Empirical EEG data**

### 187 **2.3.1 Participants**

188 Sixty-three right-handed (Edinburgh Handedness Inventory; Oldfield, 1971), native English-speaking adults  
189 (42 females, mean age = 35 years, range = 18–74 years) with normal (or corrected-to-normal) vision and  
190 audition, and no history of psychiatric, neurological, or cognitive disorder, participated in the study. All  
191 participants provided written, informed consent, and were remunerated for their time. This study was part of a  
192 larger research project investigating EEG responses to complex, naturalistic stimuli, and was approved by the  
193 University of South Australia Human Research Ethics Committee (Application ID: 0000035576).

### 194 **2.3.2 Procedure**

195 Participants were seated in a dimly-lit, sound-attenuated room for the duration of the session (2.5–3 hr). Two  
196 sets of resting-state EEG recordings were acquired approximately 90 min apart at the beginning and end of an  
197 experimental procedure. This experiment involved watching approximately 70 min of prerecorded television  
198 programming, followed by an old/new cued recall task. As per our standard laboratory protocol, both sets of  
199 resting-state recordings comprised approximately 2 min of eyes-open EEG followed by 2 min of eyes-closed  
200 EEG. Participants were instructed to sit still, relax, and avoid excessive eye movements during this time.  
201 Note, only data from the eyes-closed component of the resting-state recordings are analysed here. We favour  
202 eyes-closed resting-state data on the basis that it demonstrates (1) greater interindividual variability in alpha  
203 power (Chen, Feng, Zhao, Yin, & Wang, 2008), and (2) higher within-session reliability and test-retest stability  
204 of IAF estimates (Grandy et al., 2013b) than eyes-open data. Eyes-closed recordings may also be advantageous  
205 in reducing ocular artifact.

### 206 **2.3.3 EEG acquisition and preprocessing**

207 EEG was recorded continuously from 64 cap-mounted Ag/AgCl electrodes via Scan 4.5 software for the  
208 SynAmpsRT amplifier (Compumedics<sup>®</sup> Neuroscan<sup>™</sup>, Charlotte, NC, USA). The online recording was digitised  
209 at a rate of 1000 Hz, bandpass filtered (passband: 0.05–200 Hz), and referenced to the vertex electrode (AFz  
210 served as the ground electrode). Eye movements were recorded from bipolar channels above and below the left  
211 eye, and on the outer canthi of both eyes. Electrode impedances were maintained below 12.5 k $\Omega$ .

212 EEG data acquired from eyes-closed resting-state recordings were preprocessed in MATLAB 2015a  
213 (v8.5.0.197613). All EEG channels were imported into MATLAB via EEGLAB (v13.6.5b) and re-referenced

214 to linked mastoids. Each dataset was then trimmed to retain only the EOG and the nine centro-posterior  
215 electrodes constituting the region of interest for this analysis: Pz, P1/2, POz, PO3/4, Oz, O1/2. These  
216 channels were subjected to zero-phase, finite impulse response highpass (passband: 1 Hz, -6 dB cutoff: 0.5 Hz)  
217 and lowpass (passband: 40 Hz, -6 dB cutoff: 45 Hz), Hamming-windowed sinc filters. Automated artifact  
218 detection routines were then applied to identify regions of channel data (segmented into 2 s epochs) that  
219 contained excessive deviations in the frequency domain (frequency range: 15–40 Hz, spectral threshold: 10 dB).  
220 Channels that exhibited an improbable signal distribution (kurtosis  $z$ -score  $> 5$ ) were excluded from analysis.  
221 EOG channels were removed following artifact rejection, and remaining channels were downsampled to 250 Hz  
222 in preparation for spectral analysis. Datasets exceeding 120 s were trimmed to this duration in order to reduce  
223 variability in the quantity of data analysed per participant.

#### 224 **2.3.4 IAF analysis parameters**

225 Initial parameters for the IAF analysis were determined on the basis of preliminary testing on an independent  
226 dataset (collected as part of a separate EEG protocol). We implemented `pwelch` with a 1024 sample Hamming  
227 window (i.e. 4 times the sampling rate raised to the next power of 2; window overlap = 50%), yielding a  
228 frequency resolution of  $\sim 0.24$  Hz. SGF and peak detection parameters were defined as follows:  $F_w = 11$   
229 (corresponding to a frequency span of  $\sim 2.69$  Hz);  $k = 5$ ;  $W_\alpha = [7, 13 \text{ Hz}]$ ;  $pDiff = .20$  (meaning that the largest  
230 peak detected within  $W_\alpha$  had to be at least 20% higher than any other peak to qualify as the PAF estimate);  
231  $cMin = 3$ .  $minP$  was automatically determined for each channel spectrum according to its distributional  
232 characteristics.

### 233 **2.4 Simulated EEG data**

#### 234 **2.4.1 Single component simulations**

235 As an initial proof of concept, we analysed the performance of the SGF routine in extracting target alpha  
236 frequency components embedded within noisy time series. These composite signals were created by combining  
237 a sine wave oscillating at target frequency  $F_\alpha$  with a 2 min ‘pink noise’ signal (i.e. a randomly sampled signal  
238 with a frequency distribution scaled in accordance with the  $1/f$  inverse power-law). SNR was manipulated by  
239 varying the length of the target signal embedded in the composite time series (e.g., for SNR = 0.5, the first  
240 half of the signal would comprise the convolution of the alpha and noise signals, whereas the second half would  
241 comprise only the noise signal).

242 We examined PAF estimation at SNR = 0.05, 0.10, 0.15, 0.20, 0.25, 0.30, 0.40, and 0.50, generating 1000

243 simulated signals for each SNR level. The target frequency was randomly sampled (with replacement) from a  
244 vector ranging from 7.5 to 12.5 in iterations of 0.1. We compared the SGF routine’s capacity to extract these  
245 target peaks with a that of a simple peak detection routine designed to locate the local maximum (LM) within  
246  $W_\alpha$ . To avoid spurious estimates from suprema at the lower bound of  $W_\alpha$ , this routine evaluated whether the  
247 LM exceeded the power estimates of adjacent frequency bins (thus making it functionally equivalent to the  
248 first-derivative test).

#### 249 **2.4.2 Mixture and multi-channel simulations**

250 Next, we investigated the performance of the SGF routine under more ecologically valid spectral conditions.  
251 This involved creating alpha signals that were comprised of a set of neighbouring frequency components  
252 from different channels. We did this by sampling an ‘actual’/‘measured’ alpha frequency per channel from  
253 a truncated Gaussian distribution centered at the randomly sampled target  $F_\alpha$  (selected as for the single  
254 component simulation) for each simulated (sub)component (targets chosen uniformly from the standard alpha  
255 band, as above). The tails of the Gaussian were truncated  $\pm 2.5$  Hz from its mean/target frequency. Alpha  
256 signals were thus constructed by creating a weighted average of frequencies within this distribution; in other  
257 words, a Gaussian blur was applied to the frequency-domain signal in order to generate a mixture of alpha  
258 waves in the time domain.

259 Constructed alpha signals were again combined with random pink noise signals at a specified SNR. This time,  
260 each composite alpha signal was replicated 9 times, and combined with an independently sampled pink noise  
261 signal. This yielded a dataset of 9 synthetic ‘channels’, each comprised of identical alpha signals embedded  
262 within stochastically varying background noise. This enabled us to examine how our algorithm’s channel  
263 exclusion and averaging procedures performed under varying levels of SNR and peak dispersal.

264 As per the preliminary analysis, we compared the accuracy of SGF-generated PAF estimates against those  
265 produced by the LM procedure. For the latter, the optimisation function was applied to the mean PSD  
266 calculated for each set of simulated channel data. The simulation of broader alpha-band components also  
267 afforded the opportunity to assess the performance of the CoG estimator implemented in the SGF routine.

268 Finally, we repeated the multi-channel simulations using a set of alpha signals sampled via a bimodal Gaussian  
269 window. This analysis was designed to replicate troublesome empirical cases in which IAF calculation is  
270 complicated by the presence of a split-peak; either through poor resolution of a single underlying component,  
271 or where dominant activity across multiple alpha-generators results in overlapping frequency components. This  
272 analysis likewise investigated the effect of modulating the composition of the alpha signal, and the SNR of the

273 combined time series, on IAF estimation. As the bimodal sampling window introduced the possibility of more  
274 extreme peaks (since peaks necessarily fell either side of the window centre), the span of  $W_\alpha$  was extended to  
275 [6, 14 Hz]. This exception aside, all simulation analyses implemented the same set of parameters as described  
276 in Section 2.3.4.

## 277 3 Results

### 278 3.1 Empirical EEG data

#### 279 3.1.1 Global performance of the SGF routine

280 Post-experiment resting-state recordings were missing  
281 for 3 participants. A total of 11 channels (all from  
282 separate recordings) were excluded on the basis of  
283 excessive kurtosis. This left a total 1096 PSDs to  
284 estimate across the sample (pre = 561, post = 535).  
285 Of these, a total 944 PAF (pre = 480, post = 464) and  
286 1003 CoG (pre = 507, post = 496) estimates were ex-  
287 tracted. As Figure 2 indicates, the estimation routine  
288 extracted a high proportion of PAF and CoG esti-  
289 mates across most individuals. Two participants failed  
290 to surpass the  $cMin$  threshold for both recordings  
291 and were therefore excluded from the PAF analysis.  
292 Visual inspection of channel spectra confirmed the  
293 absence of any consistent alpha peak. The CoG was  
294 however estimated for one of these individuals.

#### 295 3.1.2 Statistical properties of IAF estimates

296 Mean IAF estimates were centred about 10 Hz, with  
297 the majority falling in the range of 9 to 11 Hz. Both  
298 estimators were similarly distributed in both sets of  
299 recordings (see Figure 3A). Intraclass correlation coefficients ( $ICC_{3,k}$ :  $PAF_M = .96$ ;  $CoG_M = .98$ ) indicated  
300 that variance in  $PAF_M$  and  $CoG_M$  estimates was predominantly attributable to interindividual differences

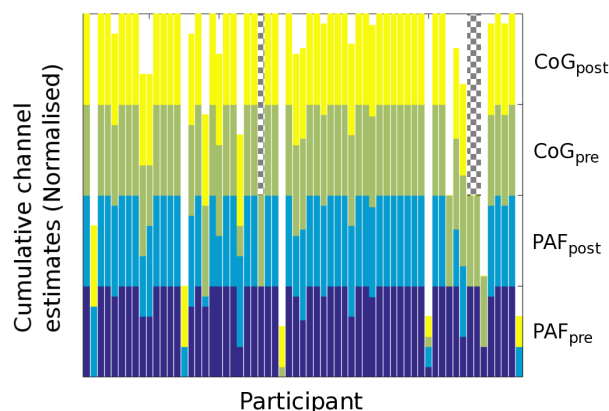


Figure 2: Stacked bar chart displaying number of channels from which PAF (lower half) and CoG (upper half) estimates were derived across participants. Estimates are further divided according to EEG recording (pre/post). Totals normalised to take into account excluded channels. Post-experiment data were unavailable for 3 participants (indicated by hatching).

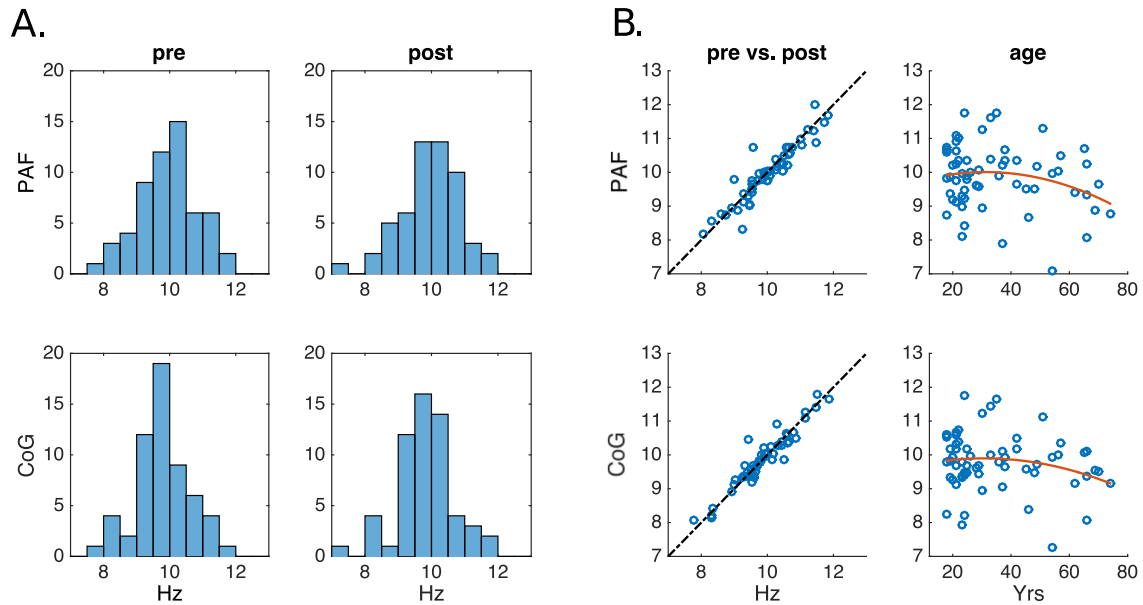


Figure 3: Statistical properties of PAF and CoG estimates. A: Histograms displaying distribution of mean PAF and CoG estimates across pre/post recordings. B: Scatterplots showing correlations between pre and post IAF estimates (left column), and grand-averaged IAF estimates as a function of age (right column). Broken line indicates perfect positive correlation. Red line indicates 2nd-degree polynomial fit.

301 across the sample, rather than intraindividual differences between recordings (see Figure 3B). These data  
 302 are therefore in accord with previous reports of the IAF's high temporal stability (at least within the same  
 303 recording session) and interindividual variability (at least in the context of eyes-closed resting-state EEG).

304 Kernel density estimation of grand-averaged alpha peak and gravity estimates ( $PAF_{GA}$  and  $CoG_{GA}$ , respectively)  
 305 suggested that the probability density function underlying both estimators was well-characterised by a Gaussian  
 306 distribution, although  $CoG_{GA}$  was rather more heavy-tailed. Despite this difference,  $PAF_{GA}$  and  $CoG_{GA}$   
 307 produced remarkably consistent results ( $ICC_{3,k} = .97$ ;  $R^2 = .90$ ). This finding, which extends that reported in  
 308 a smaller sample by Jann, Koenig, Dierks, Boesch, and Federspiel (2010), lends weight to the claim that these  
 309 two estimators tap into the same fundamental oscillatory process(es).

310 As a final point of comparison with previous findings, we examined the relation between age and IAF (Figure  
 311 3B). Both estimators showed a similar trend towards reduced IAF as age increases beyond the fourth decade.  
 312 However, this association accounted for a rather small proportion of the variance ( $R^2 = 0.05$  and  $0.04$  for  
 313  $PAF_{GA}$  and  $CoG_{GA}$ , respectively). This is consistent with previously reported findings from much larger  
 314 datasets (e.g., Chiang et al., 2011).

## 3.2 Simulated EEG data

### 3.2.1 PAF estimator performance as a function of SNR

Preliminary analysis of synthetic EEG data focused on the number of PAF estimates extracted at each SNR level, and how well these estimates approximated the ground truth stipulated by the frequency of the alpha signal embedded in the synthetic time series. The results of this analysis are summarised in Table 1.

Table 1: Summary statistics characterising PAF estimation as a function of estimation method and SNR.  $PAF_{LM}$ : PAF estimated via the local maximum detection method;  $PAF_{SG}$ : PAF estimated via the Savitzky-Golay smoothing method;  $n\ PAF$ : total number of PAF estimates extracted from 1000 simulated time series;  $RMSE$ : root mean squared error;  $maxDiff$ : maximum absolute difference between estimated and target frequency;  $binShift$ : number of estimates that diverged from their target frequency by  $> 0.24$  Hz.

SNR	0.05	0.10	0.15	0.20	0.25	0.30	0.40	0.50
<b>n PAF</b>								
$PAF_{LM}$	985	1000	1000	1000	1000	1000	1000	1000
$PAF_{SG}$	659	955	997	1000	1000	1000	1000	1000
<b>RMSE</b>								
$PAF_{LM}$	1.06	0.22	0.10	0.08	0.07	0.07	0.07	0.07
$PAF_{SG}$	0.09	0.09	0.08	0.07	0.07	0.07	0.07	0.07
<b>maxDiff</b>								
$PAF_{LM}$	5.42	4.83	0.70	0.50	0.50	0.23	0.22	0.14
$PAF_{SG}$	0.62	0.75	0.75	0.31	0.26	0.18	0.13	0.13
<b>binShift</b>								
$PAF_{LM}$	224	70	29	8	4	0	0	0
$PAF_{SG}$	7	14	3	2	1	0	0	0

The SGF technique failed to extract PAF estimates for approximately one-third of simulations at SNR = 0.05, however the proportion of estimated alpha peaks rapidly approached ceiling as SNR increased beyond 0.10. Average error ( $RMSE$ ) was generally low for all levels of SNR, suggesting that alpha peaks were consistently

323 estimated with a high degree of accuracy when detected by the SGF analysis routine. Between 1-2% of  
324 PAF estimates in the  $\text{SNR} < 0.15$  conditions deviated from their target frequencies by the equivalent of up  
325 to 3 frequency bins. Given the rareness of these *binShift* deviations in the higher SNR conditions, and the  
326 relatively low magnitude of such discrepancies when they did occur, it seems that the SGF technique exhibited  
327 near-optimal performance at  $\text{SNR} \geq 0.30$ .

328 The LM routine returned PAF estimates for all simulated spectra; however, 15 estimates in the  $\text{SNR} = 0.05$   
329 condition were discarded as lower bound suprema. Even with these estimates removed, LM detection was  
330 associated with a 12-fold increase in average estimate error in the  $\text{SNR} = 0.05$  condition as compared to the  
331 SGF method. Of the 224 estimates that were shifted by more than one frequency bin from their corresponding  
332 target frequency, 42 deviated by 1 to 2.5 Hz, while a further 56 deviated by  $> 2.5$  Hz. All of these extreme errors  
333 constituted underestimates of the target component. The LM procedure was also markedly less accurate in the  
334  $\text{SNR} = 0.10$  condition, where it registered more than double the RMSE of SGF-resolved peaks. Average LM  
335 estimation error converged with that of the SGF technique in higher SNR conditions, although the magnitude  
336 of worst errors (*maxDiff*) remained elevated relative to SGF-generated PAF estimates.

337 To give a flavour of how smoothing may have influenced the PSD estimates generated by `pwelch` at each SNR  
338 level, a selection of simulated PSD functions are illustrated in Figure 4. Both techniques return identical  
339 PAF estimates at the higher SNRs. The SGF also tends to attenuate peak height, as would be expected of  
340 a smoothing procedure. The  $\text{SNR} = 0.30$  panel reveals one instance where the application of the smoothing  
341 procedure to a reasonably blunt component results in the erroneous ascription of PAF to a neighbouring  
342 frequency bin. The advantages of the SGF technique are however thrown into relief by two scenarios where the  
343 LM estimator errs. In the  $\text{SNR} = 0.05$  panel, the LM routine identifies a spurious fluctuation at 7.57 Hz as the  
344 PAF ( $F\alpha = 9.9$  Hz). Here, the LM technique is disadvantaged by its inability to evaluate whether the detected  
345 LM constitutes a substantial deviation from background noise. The second scenario arises when the target  
346 component is suboptimally resolved by `pwelch`, resulting in either a broad structure featuring two maxima  
347 ( $\text{SNR} = 0.10$ ) or a more clearly defined split-peak ( $\text{SNR} = 0.20$ ). In both cases, smoothing helps to recover the  
348 shape of the peak component underlying the spectral data, thus culminating in more veridical PAF estimates  
349 than those derived via the LM method.

350 In sum, this preliminary analysis provides compelling evidence that the SGF method generally furnishes  
351 accurate estimates of the PAF when a singular alpha component is present within the PSD. Such accuracy is  
352 maintained even at relatively low SNR levels, although the extraction of low-powered peaks amidst background  
353 noise becomes more challenging when SNR drops below 0.15. The more conservative nature of the SGF method  
354 (as compared to LM detection) in the context of low SNR may however be advantageous in protecting against

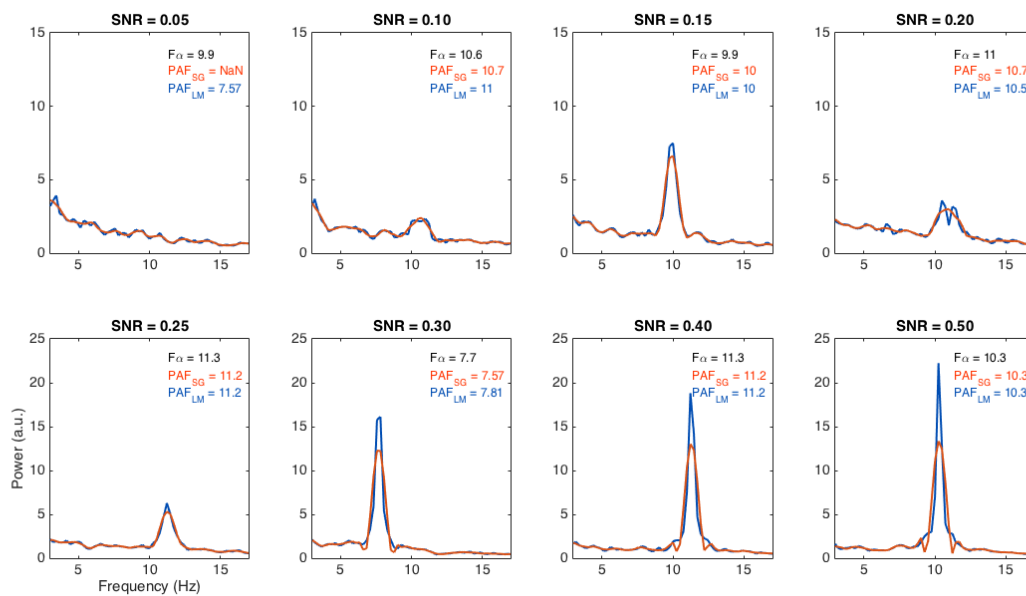


Figure 4: Channel spectra randomly sampled from each SNR condition. Blue functions represent PSD estimates generated by `pwelch`. Red functions indicate effect of smoothing these estimates with the Savitzky-Golay filter (SGF).  $F_\alpha$ : Target alpha component frequency;  $PAF_{SG}$  and  $PAF_{LM}$ : Estimates of  $F_\alpha$  rendered by the SGF and local maximum methods, respectively. *a.u.*: Arbitrary unit; *NaN*: No estimate returned.

355 inaccurate PAF estimates issuing from spurious background fluctuations.

### 356 3.2.2 Multi-channel dataset simulations

357 Given that the PAF estimators approached ceiling performance at moderate levels of SNR in the previous  
 358 analysis, we limited multi-channel simulations to a low (0.15) and a moderate (0.40) SNR condition. A total of  
 359 100 datasets, each comprising 9 synthetic EEG channels, were simulated for each level of alpha component  
 360 dispersal in both SNR conditions (yielding a total 5400 PSD estimates). The results of this analysis are  
 361 summarised in Figure 5 and Table 2.

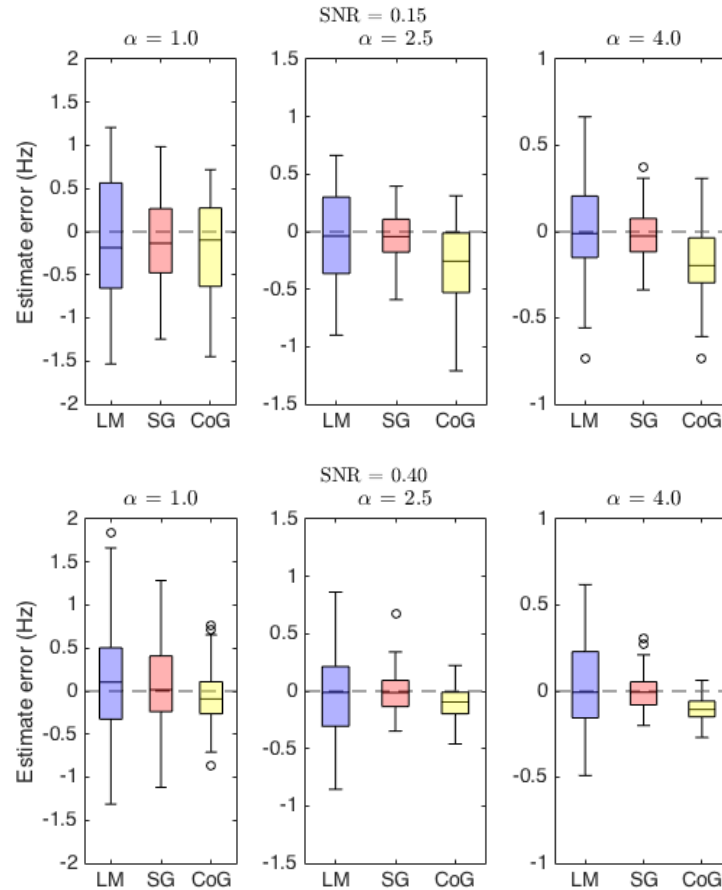


Figure 5: Box plots summarising spread of estimator error across simulation conditions. Centre marks indicate median error, edges indicate interquartile range (IQR), whiskers indicate approximately  $1.5 \times$  IQR. Zero estimate error (broken horizontal line) corresponds to extraction of the target alpha peak frequency. Negative error indicates underestimation of the target frequency, positive error indicates overestimation. Dispersal of the target alpha component broadest in the left column ( $\alpha = 1.0$ ) and narrowest in the right ( $\alpha = 4.0$ ). *LM* and *SG*: PAF estimated via the Local Maximum and Savitzky-Golay routines, respectively. *CoG*: CoG estimated via the Savitzky-Golay routine. Y-axis scaling varied across  $\alpha$  levels to aid visualisation.

Table 2: Estimator performance as a function of SNR and alpha component distribution ( $\alpha = 1.0$  corresponds to a broad peak,  $\alpha = 4.0$  a narrow peak).  $PAF_{LM}$ : Local maximum PAF estimator;  $PAF_{SG}$ : Savitzky-Golay filter (SGF) PAF estimator;  $CoG$ : SGF CoG estimator;  $RMSE$ : root mean squared error;  $maxDiff$ : maximum absolute difference between estimated and target frequency;  $\% Dev$ : percentage of estimates that diverged from the target frequency by  $> 0.5$  Hz;  $n chans$ : median (s.d.) number of channels furnishing PAF/IAW estimates per simulated dataset.

SNR	0.15			0.40		
$\alpha$	1.0	2.5	4.0	1.0	2.5	4.0
<b>RMSE</b>						
$PAF_{LM}$	0.72	0.38	0.30	0.63	0.38	0.26
$PAF_{SG}$	0.47	0.21	0.15	0.48	0.17	0.10
CoG	0.57	0.45	0.27	0.34	0.16	0.12
<b>maxDiff</b>						
$PAF_{LM}$	1.53	0.90	0.73	1.84	0.86	0.62
$PAF_{SG}$	1.24	0.59	0.38	1.29	0.68	0.31
CoG	1.45	1.21	0.73	0.86	0.46	0.27
<b>% Dev</b>						
$PAF_{LM}$	63	17	14	42	22	3
$PAF_{SG}$	30	2	0	33	1	0
CoG	42	30	7	18	0	0
<b>n chans (s.d.)</b>						
$PAF_{SG}$	5 (1.81)	6 (1.53)	8 (1.23)	5 (1.52)	7 (1.27)	9 (0.70)
CoG	9 (0.79)	9 (0.36)	9 (0.10)	9 (0)	9 (0)	9 (0)

362 Across all Distribution  $\times$  SNR conditions, the SGF routine failed to generate average PAF estimates for 11  
363 datasets. Eight of these instances occurred in the low SNR condition (7  $\alpha = 1.0$ ; 1  $\alpha = 2.5$ ), while the remainder  
364 occurred when attempting to recover broad component structures ( $\alpha = 1.0$ ) in the moderate SNR condition.  
365 By contrast, both the LM and the CoG estimators rendered estimates for all 600 simulated datasets.

366 All three estimators demonstrated consistent reductions in error as alpha component dispersal diminished  
367 (i.e. as target peaks became narrower). This finding is congruent with the intuition that, irrespective of SNR,  
368 recovery of broader component structures poses a greater challenge for automated estimation procedures  
369 than the recovery of narrower, sharper peaks. Further, there was some indication of a Distribution  $\times$  SNR  
370 interaction effect, such that error indices for a given  $\alpha$  level were more elevated in the low (as compared to  
371 the moderate) SNR condition. Although this effect was somewhat marginal (and not entirely consistent) for  
372 the PAF estimators, it was more clearly apparent for the CoG estimator. These general trends (i.e. improved  
373 estimation accuracy with decreased component dispersal and increased SNR) were mirrored by both the average  
374 (median) number of channels that contributed to PAF<sub>SG</sub> estimation, and the degree of variability (s.d.) in the  
375 number of channels retained by the SGF procedure for each set of simulations. This is to say that a higher  
376 proportion of channels rendered PAF estimates as SNR increased and peak dispersal decreased, while volatility  
377 in the number of channels selected for mean PAF/IAW estimation correspondingly declined.

378 As per the single component analysis, PAF estimates from low SNR simulations were more accurate on average  
379 when estimated with the SGF procedure. Unlike the prior analysis, however, the RMSE of PAF<sub>LM</sub> failed to  
380 converge with that of PAF<sub>SG</sub> in the moderate SNR condition (indeed, RMSE of the former was more than  
381 double that of the latter for both intermediate and narrow peak estimates). The magnitude of worst estimate  
382 errors (*maxDiff*) was likewise consistently elevated for PAF<sub>LM</sub> as compared to PAF<sub>SG</sub>-generated estimates.  
383 Perhaps most notably, PAF<sub>LM</sub> produced considerably more estimate errors in excess of  $\pm 0.5$  Hz than PAF<sub>SG</sub>  
384 (27% vs. 11%). This contrast was most stark at  $\alpha \geq 2.5$ , where the error rate associated with PAF<sub>LM</sub> was 14%  
385 (compared to  $< 1\%$  for PAF<sub>SG</sub>).

386 Comparison of SGF-generated estimates of PAF and CoG discloses an interesting interaction between estimator  
387 performance and SNR. While the PAF estimator resulted in diminished RMSEs, lower maximal deviations, and  
388 fewer estimation errors  $\pm 0.5$  Hz in the low SNR simulations, this pattern was inverted (with the exception of  
389 one RMSE value) in the moderate SNR condition. This latter result provides encouraging evidence in favour of  
390 our method's capacity to accurately localise the beginning and end of the IAW (at least when the embedded  
391 alpha signal is not too weak). Interestingly, even though the CoG performed less consistently when SNR was  
392 low, it still tended to be more reliable than the PAF<sub>LM</sub> estimator. For instance, the CoG method resulted in  
393 a 16% reduction in substantial estimate errors compared to the LM method. While CoG may therefore be  
394 more susceptible to bias than its PAF<sub>SG</sub> counterpart when channel spectra contain relatively high degrees of  
395 background noise, it may still offer tangible advantages over LM-based peak detection strategies.

### 3.2.3 Split-peak simulations

Finally, we repeated the multi-channel dataset simulations with composite signals constructed using a bimodal sampling window. This window comprised two overlapping Gaussians ( $\alpha = 2.5$ ), the right-most of which was scaled equal to, 0.25, or 0.50 times larger than its counterpart. The frequency offset between the two Gaussian peaks was equivalent to 1.6 Hz. The results of this analysis are summarised in Figure 6 and Table 3.

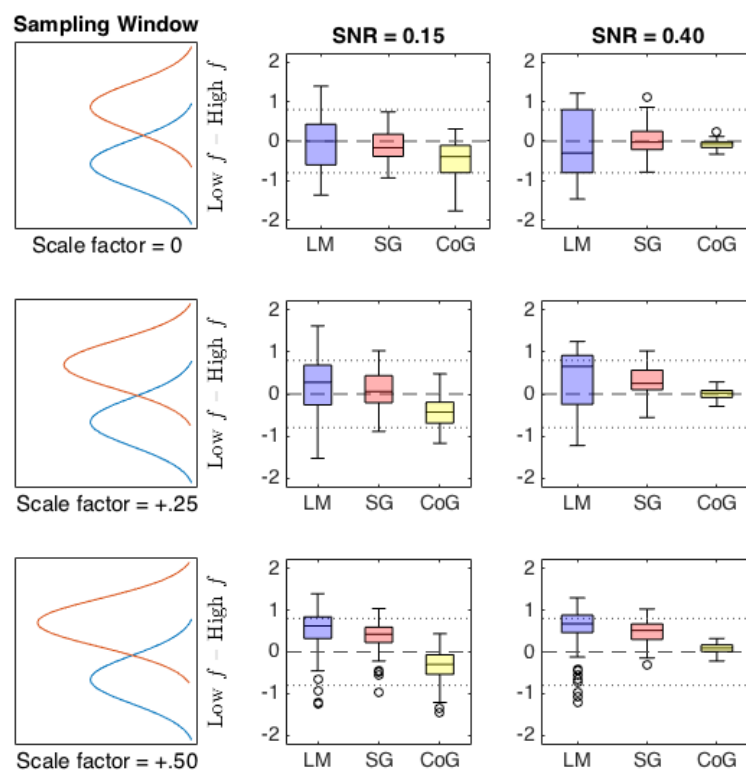


Figure 6: Box plots summarising spread of estimate deviation from the centre frequency of the sampling window. Centre marks indicate median deviation, edges indicate interquartile range (IQR), whiskers indicate approximately  $1.5 \times$  IQR. Zero deviation (broken horizontal line) corresponds to estimating the midpoint between the two components. Peak locations indicated by dotted horizontal lines. *Left column*: Schematic of the sampling window used to construct composite alpha signals simulated in corresponding row. The discrepancy between simulated peaks (higher relative to lower frequency bins) ranges from 0 (top row) to +0.50 (bottom row). *LM* and *SG*: Local Maximum and Savitzky-Golay PAF estimates, respectively. *CoG*: Savitzky-Golay CoG estimates.

Table 3: Estimator performance as a function of SNR and relative weighting of bimodal peaks. Right-most Gaussian function was either 0, 0.25, or 0.50 times larger than the left (*PeakDiff*).  $PAF_{LM}$ : Local maximum PAF estimator;  $PAF_{SG}$ : Savitzky-Golay filter (SGF) PAF estimator; *CoG*: SGF CoG estimator; *RMSE*: root mean squared error (relative to centre frequency of sampled components); *maxDiff*: maximum absolute difference between estimates and centre frequency of sampled components; *n chans*: median (s.d.) number of channels furnishing PAF/IAW estimates per dataset.

SNR	0.15			0.40		
<i>PeakDiff</i>	0	+0.25	+0.50	0	+0.25	+0.50
<b>RMSE</b>						
$PAF_{LM}$	0.69	0.69	0.75	0.84	0.79	0.76
$PAF_{SG}$	0.40	0.44	0.51	0.38	0.45	0.55
CoG	0.62	0.56	0.51	0.14	0.12	0.15
<b>maxDiff</b>						
$PAF_{LM}$	1.40	1.62	1.40	1.47	1.25	1.30
$PAF_{SG}$	0.93	1.03	1.04	1.10	1.03	1.03
CoG	1.77	1.17	1.47	0.33	0.29	0.32
<b>n chans (s.d.)</b>						
$PAF_{SG}$	4 (1.52)	5 (1.49)	5 (1.68)	5 (1.36)	6 (1.64)	6 (1.31)
CoG	9 (0.46)	9 (0.48)	9 (0.51)	9 (0)	9 (0)	9 (0)

401  $PAF_{SG}$  failed to find evidence of a distinct peak in 11% of low SNR datasets (Equal = 14, +0.25 = 7, +0.50 =  
402 11), and 2% of moderate SNR datasets (Equal = 3, +0.25 = 4, +0.50 = 0). Median number of channel PAF  
403 estimates was also reduced as compared to the corresponding SNR conditions in the single-peak, multi-channel  
404 simulations. As per the single peak, multi-channel simulations, both  $PAF_{LM}$  and CoG returned estimates for  
405 all 600 simulated datasets.

406 Across all conditions,  $PAF_{LM}$  returned more variable and extreme results than  $PAF_{SG}$ ; although interpretation  
407 of this observation is complicated by the presence of a (somewhat) dominant peak in the +0.25 and +0.50  
408 conditions. As both SNR and peak difference increase,  $PAF_{LM}$  shows stronger migration towards the higher

409 frequency peak than either of the SGF estimators, although note that it is still more prone to erroneously  
410 ascribing the PAF to the secondary (lower frequency) peak. On the other hand,  $PAF_{SG}$  is less liable to  
411 spurious fluctuations in the PSD, tending instead to curb PAF estimation towards the centre mass of the  
412 double component. This might suggest that marginal local maxima are absorbed within the recapitulation of a  
413 broader peak structure as a consequence of spectral smoothing. As SNR and peak inequality increase,  $PAF_{SG}$   
414 estimates cluster in closer proximity to the dominant peak. This then explains why RMSE increases relative to  
415 the centre frequency: as SNR improves and the split-peak becomes more asymmetrical (and hence, one peak  
416 more dominant over its competitor), more evidence accrues in favour of an underlying PAF.

417 The CoG estimator demonstrates an intermediate level of variability compared to the PAF estimators under  
418 low SNR conditions, but is markedly less variable under moderate SNR conditions. The box plots in Figure  
419 6 also indicate that the CoG estimator performed similarly across the different degrees of peak inequality  
420 within each SNR level. Irrespective of peak scaling, CoG estimates were substantially more precise when SNR  
421 = 0.40. Indeed, compared to the other two estimators, CoG is both remarkably stable and closely centred  
422 around the centre frequency of the window function. As such, this finding provides compelling evidence that  
423 our implementation of the CoG estimator renders an accurate summary of the underlying alpha component  
424 distribution.

## 425 4 Discussion

426 We have proposed a novel method for estimating the two most prevalent indices of individual alpha frequency  
427 (IAF) in the literature. This method pairs a common approach to the automated detection of local maxima  
428 (i.e. searching for first derivative zero crossings) with a well established method of resolving spectral peaks  
429 (i.e. Savitzky-Golay filtering) to derive an estimate of peak alpha frequency (PAF). It also extends the logic of  
430 the first-derivative test to estimate the bounds of the alpha peak component, thus enabling calculation of the  
431 alpha-band centre of gravity (CoG). Like other automated curve-fitting algorithms reported in the literature  
432 (e.g., Chiang et al., 2008; Lodder & Putten, 2011), this method addresses key limitations of visual PSD analysis  
433 (e.g., proneness to subjective bias, inefficiency, and poor replicability), while improving upon alternative  
434 automated approaches that may be prone to various artifacts (e.g., failure to differentiate a single dominant  
435 peak from competing spectral peaks or spurious fluctuations, reliance on alpha-band reactivity). Unlike these  
436 algorithms, however, our method is openly accessible and easy to integrate within existing MATLAB and  
437 Python-based analysis pipelines.

438 Our results demonstrate that the SGF technique can extract a high proportion of IAF estimates from an empirical

439 dataset, and that the sample-wide properties of these estimates (intraindividual stability, interindividual variance,  
440 etc) are consonant with prior reports in the literature. Furthermore, application of the technique to simulated  
441 datasets verified its ability to render accurate estimates of peak location, even under highly degraded SNR  
442 conditions. When extended to more complex simulations, the SGF technique was shown to recover target  
443 values with greater precision than an alternative peak detection method. We begin by considering the key  
444 findings of our analyses, before reflecting on present limitations and potential directions for future research.

#### 445 **4.1 Estimation of IAFs from an empirical EEG dataset**

446 Savitzky-Golay filtering of `pwelch`-generated PSD functions resulted in the extraction of a rather impressive  
447 number of IAF estimates from a moderate-sized dataset. This suggests our technique offers substantive benefits  
448 in terms of data retention in comparison to subjective analysis, which can result in high rates of attrition if  
449 dominant peaks cannot be confidently distinguished from background noise (e.g. Bornkessel-Schlesewsky et al.,  
450 2015). We note also that our SGF method furnished a higher proportion of PAF estimates than that produced  
451 by the Gaussian curve-fitting procedure implemented by Haegens and colleagues (2014). It may be the case  
452 that our non-parametric approach, which attempts to smooth the PSD rather than fit a specified function to it,  
453 retains more data by virtue of its capacity to accommodate a broader range of alpha-band distributions.

454 By the same token, it is reassuring that neither of the two cases in which the technique failed to extract  
455 PAF estimates demonstrated compelling evidence of any concerted alpha peak activity on visual inspection  
456 of their respective PSD plots. It is also worth pointing out that the diverse age range of participants within  
457 this study is likely to have posed a nontrivial challenge to any automated alpha-band quantification routine,  
458 given the typically reported changes in both spectral power and distribution associated with older adulthood  
459 (e.g., Dustman, Shearer, & Emmerson, 1999). That our technique was able to extract estimates for the vast  
460 majority of sampled individuals, and that it did so using a fixed set of parameters defined a priori on the basis  
461 of preliminary testing in an independent dataset, speaks to its capacity to derive resting-state IAF estimates  
462 across a broad spectrum of the healthy population.

463 Comparison of grand-averaged PAF and CoG estimates revealed a high degree of intercorrelation, despite  
464 certain differences in their distribution. Although this might prompt concerns of redundancy, we interpret  
465 this finding positively: the CoG seems to tap into a similar underlying neural process (or set of processes)  
466 as the PAF. Although not necessary in the present analysis on account of the high proportion of PAFs that  
467 were extracted across participants, this finding suggests that the CoG estimator might warrant deployment  
468 as an alternative marker of IAF in cases where the PAF cannot be obtained. In any case, given the dearth  
469 of research directly comparing these two measures (most IAF-related research involves some variant of PAF,

470 perhaps on account of the additional complexities involved in calculating the CoG), we suggest it would be  
471 informative if investigators adopted the policy of reporting both indices in parallel. Should it be the case that  
472 PAF and CoG track one another almost identically, then only one of these measures need be selected for the  
473 remaining analysis (see for e.g., Jann et al., 2010). However, if it turns out that PAF and CoG diverge under  
474 certain circumstances, delineating such cases might help improve our understanding of the IAF (and alpha-band  
475 dynamics more generally). It is of course a notable advantage of our method that it enables investigators to  
476 rapidly derive sample-wide estimates of PAF and CoG simultaneously, thus furnishing a convenient means of  
477 estimator comparison. To the best of our knowledge, no previously reported automated technique provides this  
478 functionality.

## 479 **4.2 Estimation of simulated IAFs**

480 Our preliminary simulation analyses indicated that the SGF technique approached an optimal level of per-  
481 formance when 2 min synthetic signals featured approximately 36 s of alpha-band oscillations ( $\text{SNR} = 0.30$ ).  
482 Indeed, the peak detection routine performed reasonably well when signals contained as little as 12 s of  
483 alpha-band activity, with fewer than 6% of simulated alpha components undetected or erroneously estimated  
484 by more than one frequency bin.

485 Interestingly, our analysis shows that less sophisticated approaches to peak estimation can result in substantial  
486 error at comparably low levels of SNR. It is likely that most of these inaccurate estimates derived from spurious  
487 local maxima occurring due to fluctuations in background spectral activity. Indeed, the LM method's propensity  
488 to underestimate PAF in low SNR conditions supports this interpretation, since the inverse power-law (which  
489 is not generally taken into account by LM detection methods) increases the probability of spurious local  
490 maxima at lower frequencies within the search window. Such artifacts are undesirable not only for the obvious  
491 reason that they introduce additional noise into IAF-related analyses, but also insofar as such errors diminish  
492 confidence in automated analysis methods (after all, such errors would presumably have been avoided had  
493 spectral data been subjected to visual inspection). Indeed, we consider it preferable that an automated peak  
494 detection routine should reject spectra showing inconclusive evidence of any concerted alpha-band activity,  
495 rather than generate highly deviant estimates of the underlying (albeit weak) signal. It is a strength of the  
496 SGF technique, then, that it applies more stringent criteria in the evaluation of candidate peaks.

497 In addition to demonstrating that the SGF technique performs consistently well in low-to-moderate SNR  
498 conditions, our analysis also confirmed that the application of this smoothing procedure did not cause excessive  
499 distortion of PAF estimates. Furthermore, our analysis highlighted that discrete Fourier analysis methods  
500 (such as Welch's modified periodogram) might precipitate artifactual split-peaks, and that such cases can be

ameliorated by means of a smoothing procedure. Consequently, the single component simulation analysis stands as a basic proof of concept that the SGF method is capable of (1) extracting a high proportion of underlying peak frequencies without introducing systematic bias, and (2) improving upon existing techniques of peak resolution and estimation, thus helping to maximise the number of IAF estimates that can be extracted from a given dataset. We acknowledge however that the estimation of sharply defined, single frequency alpha components may well be unrepresentative of genuine electrophysiological data in many contexts. While it is encouraging then that the SGF technique performed well under these reasonably favourable conditions, it was necessary to demonstrate its capabilities when confronted with more complex, ecologically valid signals.

The multi-channel simulation analyses were designed to be more faithful to empirical resting-state EEG data, in as much as each target signal comprised a range of alpha components embedded within a variety of nonidentical (but highly correlated) time series. These simulations also enabled us to examine the performance characteristics of the SGF routine's CoG estimator, which was expected to closely approximate the PAF in the context of Gaussian-distributed alpha components. The critical finding across all simulation conditions was that the SGF technique rendered PAF and CoG estimates that almost always improved upon LM-derived PAF estimates from averaged channel spectra. This finding held irrespective of whether estimator deficits were quantified in terms of the average error across simulated datasets, magnitude of worst (i.e. most deviant) estimate errors, or percentage of estimates in the dataset that deviated from the ground truth by more than  $\pm 0.5$  Hz (a threshold previously used by Lodder and Putten, 2011, to evaluate the performance of their peak detection algorithm).

Leaving aside the superiority of the SGF over the LM detection routine, one might still raise the concern that its performance falls somewhat short when applied to broadly-dispersed alpha component structures. Indeed, the RMSE of the PAF estimator in both SNR conditions of the single-peak analysis approaches the  $\pm 0.5$  Hz threshold demarcating substantial estimate deviation, while the CoG exceeds this limit when SNR is low. Correspondingly, low- $\alpha$  multi-channel simulations returned a much higher proportion of estimates exceeding the  $\pm 0.5$  Hz error threshold (as compared to simulations involving higher  $\alpha$  levels), especially in the case of the PAF estimator. It ought to be borne in mind, however, that all simulation analyses were performed using SGF parameters identical to those used in the empirical analysis. This is pertinent because it is likely that the filter frame width ( $F_w = 11$ ) was suboptimally narrow for the purpose of smoothing such broad peak structures. Indeed, post hoc analysis (not reported) revealed that simply doubling the length of the filter frame can halve the number of simulations that failed to produce PAF estimates, as well as reducing substantial estimate deviation by one third under moderate SNR conditions. Corresponding improvements were not realised however in the context of low SNR; hence, the recovery of broadly dispersed, relatively weak alpha signals remains technically challenging.

533 Of the three IAF estimators examined in these simulations, the CoG was most sensitive to manipulation  
534 of the SNR. That low SNR simulations should inflict notable performance decrements is hardly surprising,  
535 however, given that CoG calculation depends upon the spectral characteristics of the entire (individualised)  
536 alpha-band interval across all available channels. Not only does low SNR pose nontrivial difficulties in defining  
537 the bounds of the alpha interval (thus threatening to introduce noise by either including extraneous data from  
538 beyond the alpha interval, or excluding portions of the alpha band from analysis), the relative weakness of  
539 the alpha signal means that a higher proportion of background noise contributes to CoG calculation. This  
540 scenario may be compounded by the fact that the traditional method of computing CoG estimates averages  
541 across all available channels, not just those that contributed to calculation of the IAW (although note that  
542 the average number of channels selected to infer this bandwidth remained high even in the doubly challenging  
543 conditions posed by the low SNR  $\times$  broad component dispersal combination of the single-peak analysis). It  
544 might be the case then that the central tendency-like properties of the CoG, which may have underpinned its  
545 strong performance in the moderate SNR simulations (where, of the three estimators, it was the least prone to  
546 substantial estimate deviation), render it more vulnerable to error when substantive alpha-band activity is  
547 relatively sparse. Consequently, it could be useful to investigate whether the performance of the CoG estimator  
548 in relatively noisy conditions can be augmented through the development of more robust methods of calculation.

549 Taking the results of the single- and split-peak simulations together, it is tempting to conclude that the PAF  
550 estimator outperforms its CoG counterpart in the former scenario, while the opposite is true in the latter.  
551 Even under relatively favourable spectral conditions, the CoG estimator tended to underestimate the target  
552 frequency in the single-peak simulations. Indeed, CoG estimates increasingly deviated from the centre frequency  
553 of the target component as the latter became narrower, which seems counterintuitive if such peaks ought to be  
554 less difficult to resolve and parameterise. We suggest however that this tendency derived from the skewness  
555 introduced into the Gaussian-distributed target components when they were combined with the pink noise  
556 signal. This observation thus reinforces the point that PAF and CoG estimators summarise different features  
557 of the spectral distribution, and that they need not always converge. Analysis of the split-peak simulations  
558 suggests however that the SGF method may still be somewhat prone to PAF estimate distortion when the  
559 underlying `pwelch` routine fails to consistently resolve dual subcomponents across channel spectra. This finding  
560 suggests a more stringent *cMin* criterion might be advisable to avoid PAF estimates that might in fact reflect  
561 a more CoG-like average across channels that, due to random noise fluctuations, resolve only one of two (or  
562 more) underlying subcomponents. In our view, the fact that the SGF approach to PAF estimation does not  
563 fully eliminate the methodological and conceptual challenges posed by split-peaks is not so much an intrinsic  
564 shortcoming of our technique in particular, but reflects rather a problematic attribute of the PAF in general.  
565 These data thus lend weight to the argument that the CoG, insofar as it avoids these difficulties, might be

566 preferable to the PAF.

### 567 **4.3 Limitations and future developments**

568 We aimed to design an accessible, fast, automated routine that calculates reliable PAF and CoG estimates from  
569 posterior channel EEG data recorded during short periods of relaxed, eyes-closed wakefulness. Although limited  
570 in its current scope, we believe that the programme could be adapted for application across a broader range  
571 of empirical contexts (e.g., quantifying spectral dynamics across various frequency bands during task-related  
572 activity; quantifying peak characteristics across different topographical regions). It may prove more challenging,  
573 however, to accurately resolve estimates of IAF under conditions that are less conducive to the manifestation  
574 of a dominant alpha peak (or indeed, in populations known to manifest spectral characteristics that differ from  
575 those of neurotypical adults). Further research would therefore be required to establish the utility of the SGF  
576 technique for applications beyond the rather circumscribed conditions examined here.

577 One aspect of performance that was not investigated in our analysis was whether the accuracy and precision of  
578 IAF estimates depend upon the method used to derive underlying PSD estimates. In its present implementation,  
579 our algorithm relies upon Welch's method to estimate the PSD that is subjected to the SGF's smoothing and  
580 differentiation operations. It may therefore be worthwhile to investigate whether alternative methods of PSD  
581 estimation (e.g., the multitaper method, continuous wavelet transform) can be exploited in conjunction with  
582 the SGF technique in order to further improve IAF estimation.

583 Another possible avenue for optimising the performance characteristics of the SGF routine would be to develop  
584 a function that automatically adapts the  $F_w$  (filter width) and  $k$  (polynomial degree) parameters in accordance  
585 with the approximate span of the dominant frequency component located within the search window  $W_\alpha$ .  
586 This would involve implementing an iterative fitting process, where the empirical features of the alpha-band  
587 component are initially parameterised in order to scale  $F_w$  and  $k$ . Once these parameters have been determined  
588 for the data at hand, smoothing and estimation procedures would proceed as described above.

589 Finally, it would be desirable to create a package that incorporates the MATLAB implementation of the SGF  
590 routine within the EEGLAB graphical user interface. Not only would this help to make the procedure accessible  
591 to the broadest possible range of EEGLAB users, it would also provide a convenient platform for integrating  
592 visualisations of the spectral analysis that may (for instance) assist in the diagnosis of suboptimal parameter  
593 settings. We intend to explore a number of these possibilities in future work.

## 594 **5 Conclusion**

595 We have developed a free, open-source programme for automatically estimating individual alpha frequency in  
596 resting-state EEG data. This programme has been shown to perform more accurately than a simpler automated  
597 peak detection routine, and may return a higher proportion of empirical IAF estimates than techniques relying  
598 on parametric curve-fitting procedures. Furthermore, this method is not dependent on phasic changes in  
599 alpha-band reactivity, which may produce biased IAF estimates. In addition to its obvious advantages from  
600 the perspective of replicability and efficiency, our simulations indicate that this method could help to improve  
601 the accuracy and precision of future IAF-related research. This technique may also open up new lines of  
602 methodological inquiry, insofar as it facilitates the direct comparison of two prevalent indices of IAF that have  
603 for the most part been investigated in isolation of one another.

### 604 **Acknowledgements**

605 We thank Jessica Gysin-Webster and Daniel A. Rogers for their assistance with data collection.

## References

- 606
- 607 Adrian, E. D., & Matthews, B. H. C. (1934). The berger rhythm: Potential changes from the occipital lobes in  
608 man. *Brain*, *57*, 355–385.
- 609 Albada, S. J. van, & Robinson, P. A. (2013). Relationships between electroencephalographic spectral peaks across  
610 frequency bands. *Frontiers in Human Neuroscience*, *7*(56), 1–18. <https://doi.org/10.3389/fnhum.2013.00056>
- 611 Bazanova, O. M., & Vernon, D. (2014). Interpreting eeg alpha activity. *Neuroscience & Biobehavioral Reviews*,  
612 *44*, 94–110. <https://doi.org/10.1016/j.neubiorev.2013.05.007>
- 613 Berger, H. (1929). über das elektrenkephalogramm des menschen. *Archiv Fur Psychiatrie Und Ner-*  
614 *venkrankheiten*, *87*, 527–570.
- 615 Bornkessel, I. D., Fiebach, C. J., Friederici, A. D., & Schlesewsky, M. (2004). "Capacity" reconsidered:  
616 Interindividual differences in language comprehension and individual alpha frequency. *Experimental Psychology*,  
617 *51*(4), 279–289. <https://doi.org/10.1027/1618-3169.51.4.279>
- 618 Bornkessel-Schlesewsky, I., Philipp, M., Alday, P. M., Kretzschmar, F., Grewe, T., Gumpert, M., . . . Schlesewsky,  
619 M. (2015). Age-related changes in predictive capacity versus internal model adaptability: Electrophysiological  
620 evidence that individual differences outweigh effects of age. *Frontiers in Aging Neuroscience*, *7*(217). <https://doi.org/10.3389/fnagi.2015.00217>
- 622 Bromba, M. U. A., & Ziegler, H. (1981). Application hints for savitzky-golay digital smoothing filters. *Analytical*  
623 *Chemistry*, *53*(11), 1583–1586.
- 624 Cecere, R., Rees, G., & Romei, V. (2015). Individual differences in alpha frequency drive crossmodal illusory  
625 perception. *Current Biology*, *25*(2), 231–235. <https://doi.org/10.1016/j.cub.2014.11.034>
- 626 Chen, A. C. N., Feng, W., Zhao, H., Yin, Y., & Wang, P. (2008). EEG default mode network in the human brain:  
627 Spectral regional field powers. *NeuroImage*, *41*(2), 561–574. <https://doi.org/10.1016/j.neuroimage.2007.12.064>
- 628 Chiang, A. K. I., Rennie, C. J., Robinson, P. A., Albada, S. J. van, & Kerr, C. C. (2011). Age trends and  
629 sex differences of alpha rhythms including split alpha peaks. *Clinical Neurophysiology*, *122*(8), 1505–1517.  
630 <https://doi.org/10.1016/j.clinph.2011.01.040>
- 631 Chiang, A. K. I., Rennie, C. J., Robinson, P. A., Roberts, J. A., Rigozzi, M. K., Whitehouse, R. W., . . .  
632 Gordon, E. (2008). Automated characterization of multiple alpha peaks in multi-site electroencephalograms.  
633 *Journal of Neuroscience Methods*, *168*(2), 396–411. <https://doi.org/10.1016/j.jneumeth.2007.11.001>
- 634 Cohen, M. X. (2017). Rigor and replication in time-frequency analyses of cognitive electrophysiology data.

- 635 *International Journal of Psychophysiology*, 111, 80–87. <https://doi.org/10.1016/j.ijpsycho.2016.02.001>
- 636 Delorme, A., & Makeig, S. (2004). EEGLAB: An open source toolbox for analysis of single-trial eeg dynamics  
637 including independent component analysis. *Journal of Neuroscience Methods*, 134(1), 9–21. [https://doi.org/10.](https://doi.org/10.1016/j.jneumeth.2003.10.009)  
638 [1016/j.jneumeth.2003.10.009](https://doi.org/10.1016/j.jneumeth.2003.10.009)
- 639 Dustman, R. E., Shearer, D. E., & Emmerson, R. Y. (1999). Life-span changes in eeg spectral amplitude,  
640 amplitude variability and mean frequency. *Clinical Neurophysiology*, 110(8), 1399–1409.
- 641 Gaál, Z. A., Boha, R., Stam, C. J., & Molnár, M. (2010). Age-dependent features of eeg-reactivity–Spectral,  
642 complexity, and network characteristics. *Neuroscience Letters*, 479(1), 79–84. [https://doi.org/10.1016/j.neulet.](https://doi.org/10.1016/j.neulet.2010.05.037)  
643 [2010.05.037](https://doi.org/10.1016/j.neulet.2010.05.037)
- 644 Gasser, T., Bächer, P., & Steinberg, H. (1985). Test-retest reliability of spectral parameters of the eeg.  
645 *Electroencephalography & Clinical Neurophysiology*, 60(4), 312–319.
- 646 Goljahani, A., D’Avanzo, C., Schiff, S., Amodio, P., Bisiacchi, P., & Sparacino, G. (2012). A novel method for  
647 the determination of the eeg individual alpha frequency. *NeuroImage*, 60(1), 774–786. [https://doi.org/10.1016/](https://doi.org/10.1016/j.neuroimage.2011.12.001)  
648 [j.neuroimage.2011.12.001](https://doi.org/10.1016/j.neuroimage.2011.12.001)
- 649 Grandy, T. H., Werkle-Bergner, M., Chicherio, C., Lövdén, M., Schmiedek, F., & Lindenberger, U. (2013a).  
650 Individual alpha peak frequency is related to latent factors of general cognitive abilities. *NeuroImage*, 79, 10–18.  
651 <https://doi.org/10.1016/j.neuroimage.2013.04.059>
- 652 Grandy, T. H., Werkle-Bergner, M., Chicherio, C., Schmiedek, F., Lövdén, M., & Lindenberger, U. (2013b).  
653 Peak individual alpha frequency qualifies as a stable neurophysiological trait marker in healthy younger and  
654 older adults. *Psychophysiology*, 50(6), 570–582. <https://doi.org/10.1111/psyp.12043>
- 655 Haegens, S., Cousijn, H., Wallis, G., Harrison, P. J., & Nobre, A. C. (2014). Inter- and intra-individual  
656 variability in alpha peak frequency. *NeuroImage*, 92, 46–55. <https://doi.org/10.1016/j.neuroimage.2014.01.049>
- 657 Hedden, T., & Gabrieli, J. D. E. (2004). Insights into the ageing mind: A view from cognitive neuroscience.  
658 *Nature Reviews Neuroscience*, 5(2), 87–96. <https://doi.org/10.1038/nrn1323>
- 659 Jann, K., Koenig, T., Dierks, T., Boesch, C., & Federspiel, A. (2010). Association of individual resting state eeg  
660 alpha frequency and cerebral blood flow. *NeuroImage*, 51(1), 365–372. [https://doi.org/10.1016/j.neuroimage.](https://doi.org/10.1016/j.neuroimage.2010.02.024)  
661 [2010.02.024](https://doi.org/10.1016/j.neuroimage.2010.02.024)
- 662 Klimesch, W. (1997). EEG-alpha rhythms and memory processes. *International Journal of Psychophysiology*,

- 663 26, 319–340.
- 664 Klimesch, W. (1999). EEG alpha and theta oscillations reflect cognitive and memory performance: A review  
665 and analysis. *Brain Research Reviews*, 29(2-3), 169–195.
- 666 Klimesch, W. (2012). Alpha-band oscillations, attention, and controlled access to stored information. *Trends*  
667 *in Cognitive Sciences*, 16(12), 606–617. <https://doi.org/10.1016/j.tics.2012.10.007>
- 668 Klimesch, W., Doppelmayr, M., & Hanslmayr, S. (2006). Upper alpha erd and absolute power: Their meaning  
669 for memory performance. In C. Neuper & W. Klimesch (Eds.), *Event-related dynamics of brain oscillations*  
670 (Vol. 159, pp. 151–165). Elsevier Science BV. [https://doi.org/10.1016/S0079-6123\(06\)59010-7](https://doi.org/10.1016/S0079-6123(06)59010-7)
- 671 Klimesch, W., Doppelmayr, M., Schimke, H., & Pachinger, T. (1996). Alpha frequency, reaction time, and the  
672 speed of processing information. *Journal of Clinical Neurophysiology*, 13(6), 511–518.
- 673 Klimesch, W., Schimke, H., & Pfurtscheller, G. (1993). Alpha frequency, cognitive load and memory performance.  
674 *Brain Topography*, 5(3), 241–251.
- 675 Klimesch, W., Schimke, H., Ladurner, G., & Pfurtscheller, G. (1990). Alpha frequency and memory performance.  
676 *Journal of Psychophysiology*, 4, 381–390.
- 677 Kondacs, A., & Szabo, M. (1999). Long-term intra-individual variability of the background eeg in normals.  
678 *Clinical Neurophysiology*, 110(10), 1708–1716.
- 679 Köpruner, V., Pfurtscheller, G., & Auer, L. M. (1984). Quantitative eeg in normals and in patients with  
680 cerebral ischemia. *Progress in Brain Research*, 62, 29–50.
- 681 Kreitman, N., & Shaw, J. C. (1965). Experimental enhancement of alpha activity. *Electroencephalography &*  
682 *Clinical Neurophysiology*, 18(2), 147–155.
- 683 Lodder, S. S., & Putten, M. J. A. M. van. (2011). Automated eeg analysis: Characterizing the posterior dominant  
684 rhythm. *Journal of Neuroscience Methods*, 200(1), 86–93. <https://doi.org/10.1016/j.jneumeth.2011.06.008>
- 685 Luo, J., Ying, K., He, P., & Bai, J. (2005). Properties of savitzky-golay digital differentiators. *Digital Signal*  
686 *Processing*, 15(2), 122–136. <https://doi.org/10.1016/j.dsp.2005.09.008>
- 687 Lykken, D. T., Tellegen, A., & Thorkelson, K. (1974). Genetic determination of eeg frequency spectra. *Biological*  
688 *Psychology*, 1, 245–259.
- 689 Malone, S. M., Burwell, S. J., Vaidyanathan, U., Miller, M. B., McGue, M., & Iacono, W. G. (2014). Heritability  
690 and molecular-genetic basis of resting eeg activity: A genome-wide association study. *Psychophysiology*, 51(12),

691 1225–1245. <https://doi.org/10.1111/psyp.12344>

692 Näpflin, M., Wildi, M., & Sarnthein, J. (2007). Test-retest reliability of resting eeg spectra validates a statistical  
693 signature of persons. *Clinical Neurophysiology*, *118*(11), 2519–2524. [https://doi.org/10.1016/j.clinph.2007.07.](https://doi.org/10.1016/j.clinph.2007.07.022)  
694 022

695 Noachtar, S., Binnie, C., Ebersole, J., Mauguière, F., Sakamoto, A., & Westmoreland, B. (2004). A glossary of  
696 terms most commonly used by clinical electroencephalographers and proposal for the report form for the eeg  
697 findings. *Klinische Neurophysiologie*, *35*(1), 5–21. <https://doi.org/10.1055/s-2003-812583>

698 Oldfield, R. C. (1971). The assessment and analysis of handedness: The edinburgh inventory. *Neuropsychologia*,  
699 *9*, 97–113.

700 Press, W. H., Teukolsky, S. A., Vetterling, W. T., & Flannery, B. P. (1992). Numerical recipes in fortran 77:  
701 The art of scientific computing. In (2nd ed., Vol. 1). New York: Cambridge University Press.

702 Pritchard, W. S. (1992). The brain in fractal time: 1/f-like power spectrum scaling of the human electroen-  
703 cephalogram. *International Journal of Neuroscience*, *66*(1-2), 119–129.

704 Rihs, T. A., Michel, C. M., & Thut, G. (2007). Mechanisms of selective inhibition in visual spatial attention  
705 are indexed by alpha-band eeg synchronization. *European Journal of Neuroscience*, *25*(2), 603–610. <https://doi.org/10.1111/j.1460-9568.2007.05278.x>

707 Salthouse, T. A. (2011). Neuroanatomical substrates of age-related cognitive decline. *Psychological Bulletin*,  
708 *137*(5), 753–784. <https://doi.org/10.1037/a0023262>

709 Samaha, J., & Postle, B. R. (2015). The speed of alpha-band oscillations predicts the temporal resolution of  
710 visual perception. *Current Biology*, *25*(22), 2985–2990. <https://doi.org/10.1016/j.cub.2015.10.007>

711 Savitzky, A., & Golay, M. J. E. (1964). Smoothing and differentiation of data by simplified least squares  
712 procedures. *Analytical Chemistry*, *36*(8), 1627–1639.

713 Schafer, R. W. (2011). What is a savitzky-golay filter? *IEEE Signal Processing Magazine*, *28*(4), 111–117.  
714 <https://doi.org/10.1109/MSP.2011.941097>

715 Smit, C. M., Wright, M. J., Hansell, N. K., Geffen, G. M., & Martin, N. G. (2006). Genetic variation of  
716 individual alpha frequency (iaf) and alpha power in a large adolescent twin sample. *International Journal of*  
717 *Psychophysiology*, *61*(2), 235–243. <https://doi.org/10.1016/j.ijpsycho.2005.10.004>

718 Surwillo, W. W. (1961). Frequency of the 'alpha' rhythm, reaction time and age. *Nature*, *191*(479), 823–824.

719 Surwillo, W. W. (1963). Relation of simple response time to brain-wave frequency and the effects of age.

720 *Electroencephalography & Clinical Neurophysiology*, 15(1), 105–114.

721 Vogel, W., & Broverman, D. M. (1964). Relationship between eeg and test intelligence: A critical review.

722 *Psychological Bulletin*, 62(2), 132–144.

723 Welch, P. D. (1967). The use of fast fourier transform for the estimation of power spectra: A method based on

724 time averaging over short, modified periodograms. *IEEE Transactions on Audio and Electroacoustics*, AU15(2),

725 70–73.

726 Ziegler, H. (1981). Properties of digital smoothing polynomial (dispo) filters. *Applied Spectroscopy*, 35(1),

727 88–92.